Controlling the growth of single crystal ZnO nanowires by tuning the atomic layer deposition parameters of the ZnO seed layer

Alejandro Galan-Gonzalez[*1, 2], *Andrew Gallant*[2, 3], *Dagou A. Zeze*[2, 3], *Del Atkinson**[1]

1. Department of Physics, Durham University, South Rd, Durham, DH1 3LE, UK

2. Department of Engineering, Durham University, South Rd, Durham, DH1 3LE, UK

3. ITMO University, St. Petersburg, 197101, Russia

Corresponding author

*alejandro.galan@durham.ac.uk

*del.atkinson@durham.ac.uk

Abstract

Semiconducting nanowires (NWs) offer exciting prospects for a wide range of technological applications. The translation of NW science into technology requires reliable high-quality large volume production. This study provides an in-depth investigation of the parameters using an atomic layer deposition (ALD) system to grow zinc oxide (ZnO) seed layers followed by the chemical bath deposition of ZnO nanowires (NWs) to demonstrate the low-cost production of uniform single crystal wurtzite

phase ZnO NWs that is scalable to large area substrates. The seed layer texture and the morphology of the NWs grown were systematically investigated using atomic force microscopy (AFM) as a function of the seed layer deposition parameters. It is shown that the NWs growth orientation can be controlled by tuning the seed layer deposition parameters while maintaining the same chemical bath deposition conditions. Likewise, the diameters and the surface densities of the NWs varied from 23 to 56 nm and 40 to 327 NWs/μm^2, respectively. Significantly, the relationship between the seed layer structure and the NW density indicates a clear correlation between the density of seed layer surface features and the resulting surface NW density of nanowires grown.

Keywords: nanowire, zinc oxide, atomic layer deposition, seed layer, topography, roughness, seed density

Introduction

One-dimensional (1D) oxide semiconductors offer a wide range of opportunities that are fundamental to the development of novel and current electronic devices and functionalities[1]. Among these, zinc oxide[2] (ZnO) is one of the archetypal materials due to its physical and electronic properties[3] and the different 1D nanostructures[4-5] in which it has been synthesized such as nanotubes,[6-7] nanobelts,[8] nanoplatelets[9] and nanowires[10-12] (NWs). NWs are often most interesting due to their high aspect ratio and electronic properties.[13] ZnO NWs have been considered for a wide variety of applications, including water purification treatment,[14-15] gas sensors,[16-18] photovoltaic solar cells[19-20] and photocatalysis.[21-23] These applications have a variety of specific structural and functional requirements which typically include uniformity in the length and diameter of the NWs, vertical orientation from a substrate and often specific electronic functionality that is associated with single crystal structure. For technological applications, these constraints must be controlled to produce large quantities of high-quality arrays of uniform NWs with the desired dimensions and functional

characteristics at reasonable production costs and throughput. NWs can be obtained *via* gas phase and solution-based processes. Gas phase techniques, such as chemical vapour deposition[24] (CVD) or molecular beam epitaxy[25] (MBE) are characterized by the use of high temperatures, high or ultra-high vacuum and lithographically patterned catalysts to grow uniform arrays of single crystal vertical nanowires on suitable substrates. The throughput, cost and scalability of these techniques are challenging for industrial scale applications since they require significant costs in terms of growth facilities, production time and energy. In contrast, liquid phase growth[2] methods are potentially cheaper and easier to scale up. The core challenge with these methods is to control the growth processes to produce high quality homogeneous arrays of NWs. ZnO NWs are commonly grown in liquid phase by chemical bath deposition[26-27] (CBD), which is a method commonly used to deposit thin films and nanomaterials and is characterized for being a simple, cheap and reproducible process. In the particular case of ZnO NWs CBD, a ZnO seed layer is required, low temperatures (around 90°C) and atmospheric pressure are used and it can yield high quality single crystal NWs. [10, 28-30] Extensive studies on the effect of different CBD conditions have been already discussed in the literature.[9, 19, 31] Significantly, the orientation of the as-grown NWs with respect to the growth substrate and, to a certain extent, their size, are dependent on the structural properties of the seed layer. However, understanding the role of this important component of the production process has received little systematic research.

The deposition of a ZnO seed layer requires a technique that allows the deposition of high quality textured films with tuneable properties to be deposited in a short amount of time, making this process suitable for low-cost high throughput growth of the NWs. To achieve this, there are various methods such as a sputtering,[30] spin-coating[32] or atomic layer deposition[33-35] (ALD). ALD is a deposition technique based on the self-limiting chemical reactions[36] of an organometallic precursor (*e.g.* diethylzinc, for ZnO) and a co-reactant (typically water for oxides) that are introduced in a reaction chamber by a sequential series pulses and purges of the precursors. A single ALD cycle consists of one

set of pulses and purges of the precursors that ideally yields a single atomic layer of the desired material. ALD is traditionally used to deposit a wide variety of thin films such as oxides, alumina being one of the most prominent,[37] nitrides,[38] or metals[39]. The high degree of control that ALD offers can be exploited to control the key properties of a seed layer for the subsequent NW growth by tuning the crystal orientation, crystallite size and texture. Control of these properties is crucial to provide the tunability of the dimensions, surface orientation and surface density of the as-grown NWs. This is achievable by controlling some key deposition parameters, namely the pulse and purge times, the deposition temperature and the number of cycles of seed layer deposition. Depending on the values selected for these parameters, the seed layer deposition will be driven by either chemisorption, physisorption or an intermediate adsorption, thus leading to depositions within the ALD or CVD related regimes. To date, the research focusing on the influence of the seed layers on the growth of the NWs is scarce. Reports from Song[40], Liu[41] and Chen[42] discuss this influence for seed layers deposited using DC sputtering, while the work of Bielinski[35] and Szabó[43] explores ALD deposited seed layers. However, investigations on the combined influences of the different ALD deposition parameters are yet to be made. Furthermore, most of these works put little emphasis on the seed layer microstructure obtained through AFM, which provides an excellent source of information regarding the growth characteristics of the NWs.

This work systematically demonstrates the influence of the different seed layer deposition parameters using an ALD system on the texture and seed density and their influence on the NW growth. An in-depth study of the structural properties of the seed layers was carried out by selecting key seed layer deposition parameters. ZnO NWs were grown by solution-based chemical synthesis from the seed layers, a process compatible with large area growth of interest for industrial applications. The NWs showed a single crystal wurtzite phase structure and it was proven that their growth orientation, diameter and surface density can be controlled.

Materials and methods

Fabrication of ZnO NWs by CBD

Typically, 2" Silicon (1 0 0) wafers were cleaned in a piranha solution (3:1 sulphuric acid:hydrogen peroxide), rinsed under deionized (DI) water and finally dried in a nitrogen stream at room temperature. These substrates were then diced in different part to be analyzed separately to ensure the reproducibility of the results. A ZnO seed layer was then deposited on these substrates using a Cambridge Savannah S300 atomic layer deposition system. Diethylzinc (DEZ) and water were used as the zinc precursor and oxidant respectively under a constant stream of nitrogen (10 sccm) at a base pressure of 0.2 Torr. The conditions for the seed layer deposition for the different samples are shown in Table 1. ZnO NWs were grown from the ZnO seed layer by CBD at 90°C for 2 hours in a 25 mM equimolar aqueous solution containing zinc nitrate hexahydrate and hexamethylenetetramine. These conditions were maintained for all the samples. After the synthesis, the ZnO NWs were rinsed in DI water and dried under a nitrogen stream at room temperature. All the chemicals mentioned here were bought from Sigma-Aldrich and used without any further purification.

Characterization

The properties of the seed layers were characterized by X-ray reflectivity (XRR, Bede D1 High Resolution X-Ray Diffractometer, using a monochromated Cu $K\alpha_1$ radiation (1.5406 Å)) and atomic force microscopy (AFM, Veeco Nanoman II). From AFM measurements, the topography, RMS roughness and seed density of the seed layers were obtained using the free software Gwyddion. X-ray photoelectron spectroscopy (XPS, Omicron DAR 400 X-ray source using an Mg anode and an Omicron EA 125 hemispherical analyser) studies were carried out to ensure the chemistry of the seed layers. ZnO NWs were analyzed by field emission scanning electron microscopy (FESEM, FEI Helios Nanolab 600, 5 kV) to obtain their dimensions and density using the ImageJ software. Transmission electron microscopy (TEM, JEOL 2100F FEG, 100 kV) were carried out to determine the crystallography of the

as-grown NWs. For additional information regarding the characterization of the seed layers by AFM and NWs by FESEM, see Supporting Information.

Results and discussion

Atomic layer deposition structural characterization and deposition parameters

The seed layer texture, microstructure and crystallographic orientation are the crucial factors in determining the growth features of the ZnO NWs. In this work, topography refers to the physical features of the surface of the seed layer, *i.e.* the microstructure of the seed layer. For a typical ZnO seed layer, these features are formed by granular features of different sizes. The surface structure is characterized in terms of the conventional *rms* surface roughness (Rq) and seed density, defined as the surface density of significant peak features, mostly granular features in the seed layers here studied, arising from the seed layer, per square micrometre. This surface structuring of the seed layer presents regions that act as nucleation centres for the growth of the NWs.[44] For seed layers with predominant (0 0 2) crystallographic orientation, that are textured, with a homogeneous microstructure and have low roughness, typical of a traditional ALD thin seed layer deposition close to the ALD regime, the NWs grow orthogonal to the substrate, see Figure 1a. However, an irregular surface microstructure or high surface roughness is expected from an ALD deposition that is closer to a CVD regime. The orientation of the as-grown NWs is more irregular with respect to the surface of the seed layer, as illustrated schematically in Figure 1b. It should be noted that we did not carry out any specific experiment to ascertain the specific nature (ALD or CVD) of the deposition regime. In this work, the microstructure of the seed layers was controlled to be different to that of the Si substrates used because it was found to be critical to the growth of ZnO NWs.

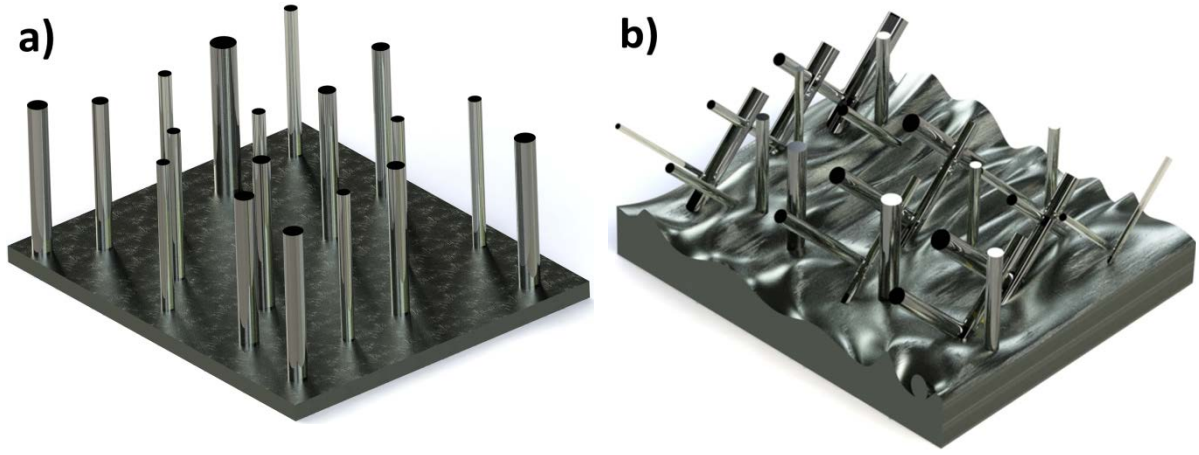

Figure 1. Schematic of vertically (a) and randomly oriented (b) as-grown NWs on a ZnO seed layer.

The seed layer deposition parameters studied in this work were the deposition temperature, the pulse and purge times of the precursors and the number of ALD cycles. These parameters were systematically studied on different sample sets, detailed in Table 1. The chemical composition of the seed layers was determined by XPS, showing pure ZnO with a small carbon (C1s) contamination in form of (see *Supporting Information* for details). Each sample set contained at least three different specimens, which were systematically analyzed to ensure the consistency of the results. For simplicity, the term 'sample' is used throughout the manuscript instead of 'sample set'. The influence of each deposition parameter on the seed layer structure and texture on the growth of NWs is detailed in the following sections.

Table 1. Summary of the sample sets studied and the associated atomic layer deposition parameters.

Sample sets	S1	S2	S3	S4	S5	S6	S7	S8
DEZ pulse (s)	0.015	0.015	0.015	0.1	1	0.1	0.1	0.1
DEZ purge (s)	20	15	5	5	5	5	5	7
Water pulse (s)	0.015	0.015	0.015	0.1	0.1	0.1	0.1	0.1
Water purge (s)	20	15	5	5	5	5	5	20
Temperature (°C)	200	250	280	280	280	280	280	280
N° cycles	250	250	250	250	250	150	500	250

ALD deposition temperature

The effect of deposition temperature on the seed layer properties was investigated in samples S1, S2 and S3 (see Table 1). S1 and S2 were within the ALD temperature window[45] (150-250°C), while S3 was above it. The purge times for samples S2 and S3 were reduced to adapt to the higher temperature. It was shown by Pung et al.,[46] that the deposition temperature controls the crystallography of the seed layer. Higher deposition temperatures (above 200°C) promote the (0 0 2) orientation as the dominant crystallographic orientation, which favors the growth of ZnO NWs orthogonal to the substrate. 280°C was selected as the deposition temperature for samples S4 to S8, which is the highest available deposition temperature on our ALD system, to ensure a predominant (0 0 2) orientation of the seed layers. The temperatures used for all samples in this work were above the 200°C threshold to ensure a predominant (0 0 2) oriented seed layer, as evidenced by the X-ray diffraction (XRD) data shown in Figure 2. Figure 2a compares the XRD spectra obtained for a ZnO seed layer and ZnO NWs. As expected from the seed layer deposition and NW growth conditions utilized, the XRD analysis shows that the NWs and the seed layers exhibit a (0 0 2) crystallographic orientation predominantly. A detailed analysis of the (0 0 2) and adjacent peaks for different seed layers is shown in Figure 2b. It is demonstrated that the (0 0 2) orientation is the dominant feature at the different deposition conditions used. In turn, small (1 0 1) contributions are observed for S1, S2 and S7, where the most significant contribution (S7) is related to the increase of the thickness of the seed layer as reported by Tian et al.[47], consistent with the increase in the number of cycles.

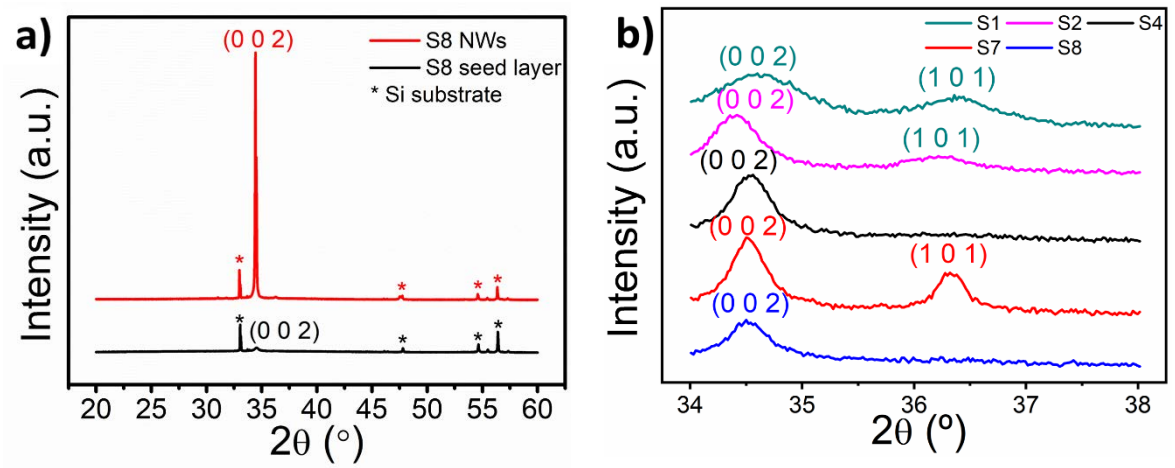

Figure 2. XRD spectra of a comparison between seed layer and NWs grown on it (a) and detail of the (0 0 2) peak for five different seed layers (b).

The microstructure and topography of the ZnO seed layers as a function of deposition temperature were investigated with atomic force microscopy (AFM). AFM images and individual line profiles are shown in Figure 3, from which it is observed that a temperature increase from 200°C (S1, Figure 3a) to 250°C (S2, Figure 3b), yields a larger surface roughness. Increasing the temperature further to 280°C (S3, Figure 3c) resulted in a seed layer formed by ZnO islands with some randomly distributed ZnO granular features, in contrast to S1 and S2 that exhibited typical seed layers deposited with an ALD system. This resulted in a lower roughness (Figure 3d), which is attributed to the use of a lower pulse time for the precursors at this high temperature. As a result, a complete adsorption of the precursors on the substrate was not allowed due to partial decomposition of the zinc precursor, meaning that the ZnO formation reactions did not fully take place. The AFM line profiles show a clear difference in terms of granular features size and microstructure. The granular features size of S1 was larger than that of S2 and S3, represented by the larger peak width from the respective line profiles. The topography of S1 and S2 was similar, with defined peaks of a similar average height. However, for S3 the peaks were narrower and lower. A comparison of the seed density as a function of deposition temperature is shown in Figure 3d, which indicates that a temperature of 250°C (S2, ~589 μm^{-2}) led to a higher seed density compared to 200°C (S1, ~201 μm^{-2}), characterized by smaller granular

features in the seed layer. However, further increasing the temperature to 280°C (S3, ~426 μm^{-2}) resulted in a lower seed density as the seed layer was not a typical ZnO seed layer deposited using an ALD system.

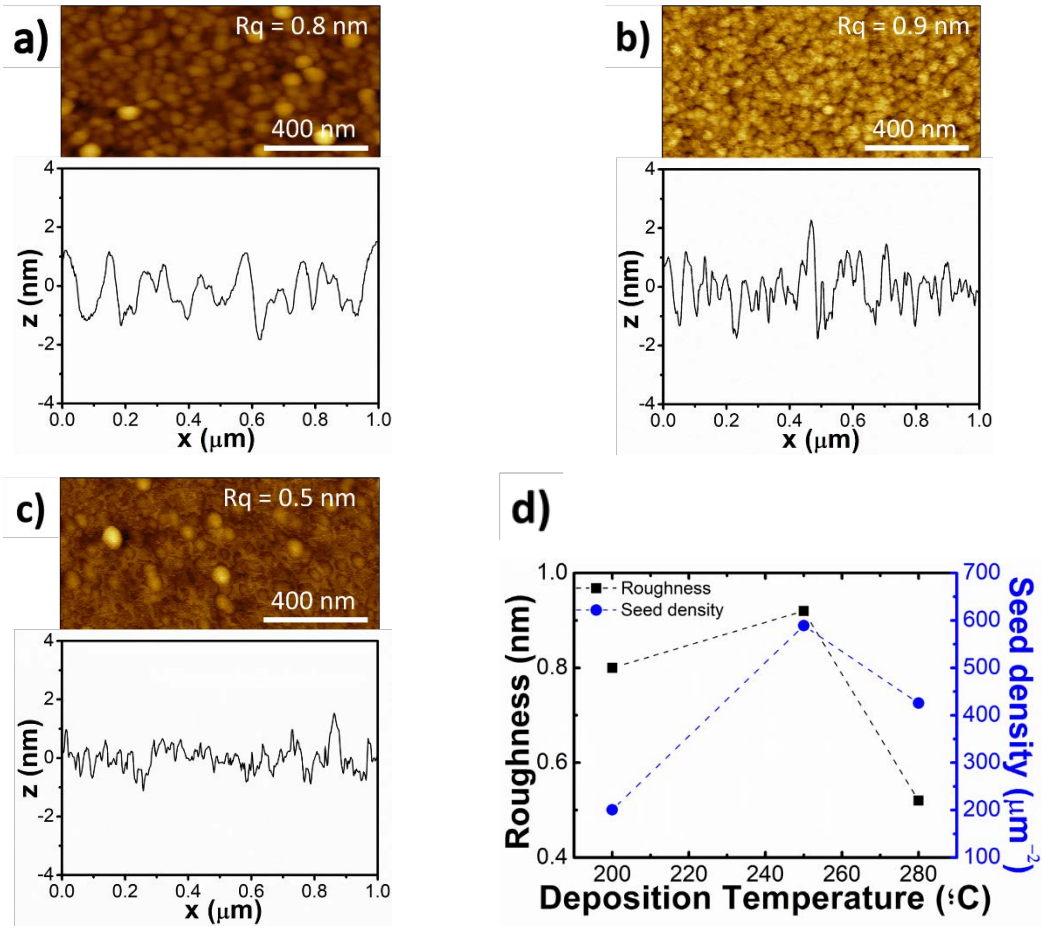

Figure 3. AFM micrographs and line profiles of (a) S1, (b) S2 and (c) S3, in which the temperature influence was studied. (d) Comparison of roughness values and seed density obtained from the AFM images.

The high-resolution field emission scanning electron microscopy (FESEM) images of the as-grown ZnO NWs are shown in Figure 4a,b,c for the NWs grown on S1, S2 and S3 respectively. Information about the NW orientation with respect to the substrate normal of the NWs was assessed from the top-view SEM images by analysing the presence or lack thereof of the lateral faces of the NWs on the top-view SEM images. As such, if only the tips were visible, the NWs were essentially vertical, while

the presence of the lateral faces indicated NWs oriented away from the vertical orientation. Comparing S1 and S2 (Figure 4a,b), it was previously shown that the increase in deposition temperature from 200 to 250°C increased the seed layer roughness while maintaining a similar topography. This translated to a slightly more disoriented arrangement of the NWs grown on S2 (250°C) compared to those grown on S1 (200°C). At the same time, the diameter of the NWs grown on S2 (22.8 nm) was less than half that of the NWs grown on S1 (55.5 nm) while the distribution of the NWs diameter grown on S1 (±10.1 nm) was notably larger than for those grown on S2 (±4.1 nm). This was correlated with a higher seed density for the higher temperature, S2, compared to S1 (Figure 3d). It is suggested that for higher seed densities, there will be a larger number of nucleation centres for NWs to grow, thus yielding a higher NW density. Additionally, a higher seed density implied smaller granular features size, which can also explain the difference in NW diameter between S1 and S2. Sample S3, prepared at 280°C, yielded NWs with a similar diameter (24.0 nm) to those in sample S2. However, the topography of this seed layer was not typical for ZnO seed layers deposited using an ALD system and the resultant orientation of the NWs grown was more variable than for S2. As a result, there was a two-fold decrease in the NW density from S2 (~327 μm^{-2}) to S3 (~163 μm^{-2}), as shown in Figure 4d. Meanwhile, due to the diameter of the NWs of S1 being more than double that of S2, the NW density was eight times smaller for S1 (~40 μm^{-2}) than for S2. It is noted that the seed (Figure 3d) and nanowire (Figure 4d) density followed a similar trend, indicating that NW nucleation is dependent on the seed density.

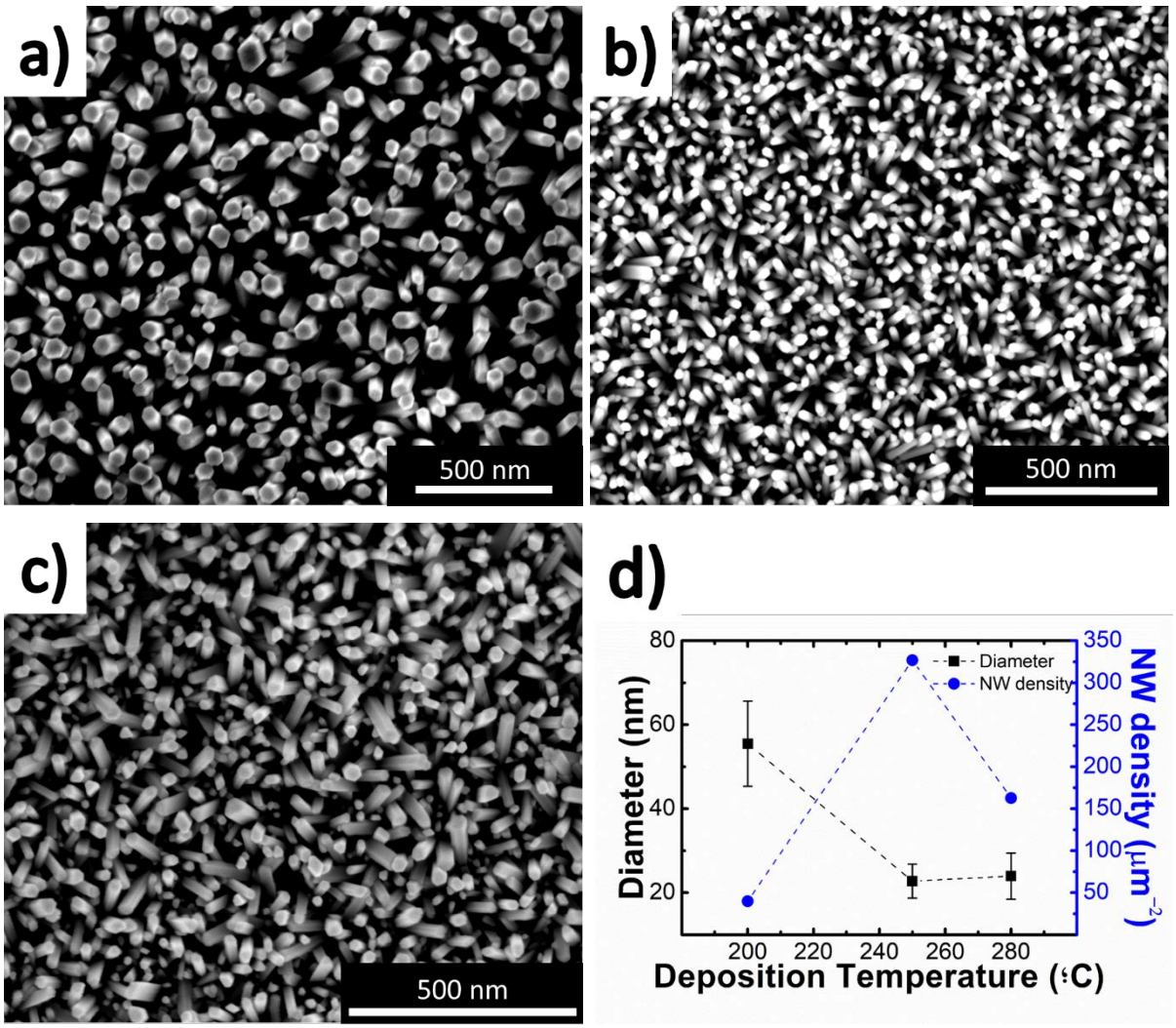

Figure 4. SEM images of the effect of temperature on the growth of ZNO NWs for samples (a) S1, (b) S2 and (c) S3. (d) Comparison of the roughness and NW density of the three samples.

Precursors pulse time

The influence of precursor pulse time on the microstructure of the seed layers was investigated in samples S4 (Figure 5a) and S5 (Figure 5b), while Figure 5c shows a comparison between the surface roughness and seed density of S3, S4 and S5. The precursor dosing, controlled by the pulse time, is critical to control the saturation of bi-products on the surface[48] and thus, the roughness and topography of the resulting seed layers. If the substrate is saturated with ethyl groups due to an excess amount of precursors (see Eq. 1), the chemisorption of DEZ is not self-limiting and deviates from an ideal ZnO seed layer deposition. This leads to undesired seed layer characteristics such as an irregular

microstructure or a non-stoichiometric seed layer composition. For sample S4 (Figure 5a), both pulse times were increased compared to S3, which yielded a typical ZnO seed layer with granular features of similar size. The roughness of this sample was high for a seed layer deposited using ALD (1.4 nm). For sample S5 (Figure 5b), only the pulse time of DEZ was increased. This led to a seed layer with lower surface roughness (0.4 nm) than S4 due to the DEZ over dosing (Figure 5c). Considering the topography of the seed layers, the line profile of S4 revealed larger granular features size compared to S5 while their topography was similar. Finally, it was shown that the seed density decreased significantly when the precursor pulse times were increased from 0.015 (S3) to 0.1 (S4) seconds (Figure 5c). This led to larger granular features. The seed density of S5 (~318 μm^{-2}) increased compared to S4 (~135 μm^{-2}).

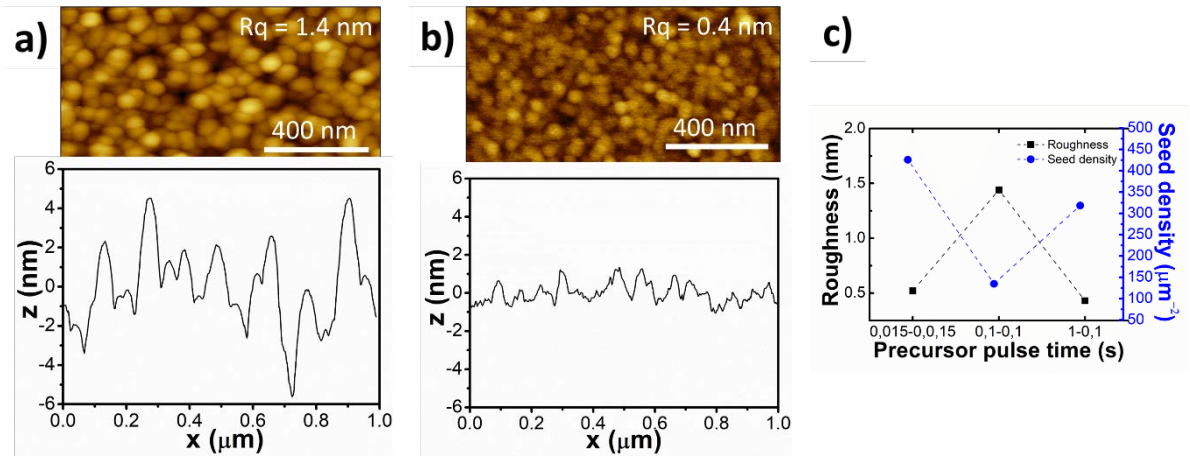

Figure 5. AFM micrographs and line profiles of samples (a) S4 and (b) S5 in which the influence of the precursors pulse time was studied. (c) Comparison of roughness values and seed density obtained from the AFM images for S3, S4 and S5.

The effect of excess Zn precursor on the seed layer was corroborated by x-ray reflectivity (XRR) measurements, Figure 6, that shows the representative XRR spectra and best fitting model spectra for S4 (Figure 6a) and S5 (Figure 6b). Comparing the values of the density from the fits to the ideal density of ZnO, 5.61 g cm^{-3}, shows that S4 (5.7 g cm^{-3}) is similar, while S5 (7.5 g cm^{-3}) is significantly larger than stoichiometric ZnO, an indication of higher Zn content in the seed layer.

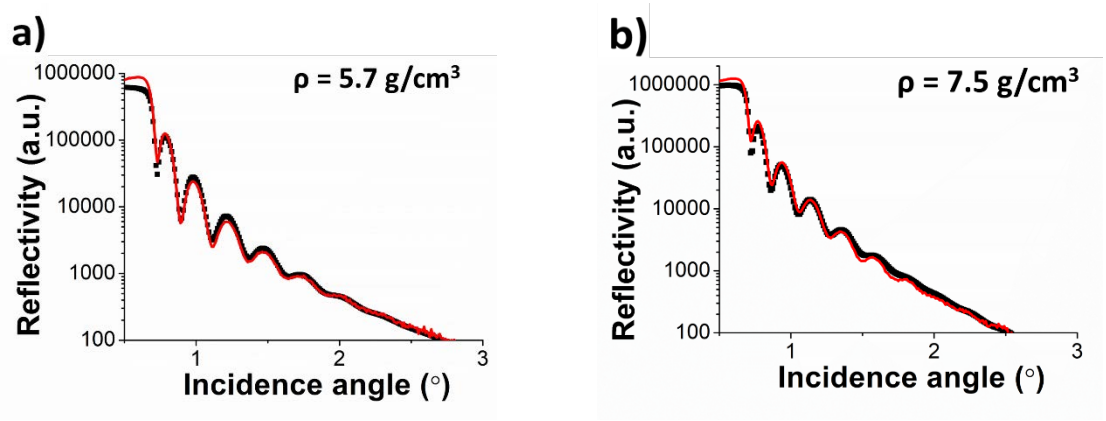

Figure 6. X-ray reflectivity spectra obtained for seed layers (a) S4 and (b) S5 from the best-fitting seed layer density values. Black symbols show experimental data while red lines indicate the best fitting simulation obtained for the data.

NWs grown on seed layers S4 and S5 are shown in Figure 7a and Figure 7b, while Figure 7c compared the NW diameter and density for the NWs grown on S3, S4 and S5. The NWs on S4 grew with random orientations, varying significantly from vertical due to the high surface roughness of the seed layer (1.4 nm). When comparing with S3, the random NW orientations combined with the larger size of the NWs led to a lower density of NWs. Finally, the size distribution for these NWs was large. The diameters of the NWs grown on S5 were smaller than those on S4 (27.0 nm and 49.4 nm respectively) as a result of a smaller granular features size of the seed layer and the NW density for S5 was increased compared to S4. Comparing the seed and NW density shows that both followed the same trend for the different precursor pulse times, indicating a relationship between nucleation of NWs and seed density. This means that the NW density increased from ~66 μm^{-2} to ~106 μm^{-2} for S4 and S5, respectively.

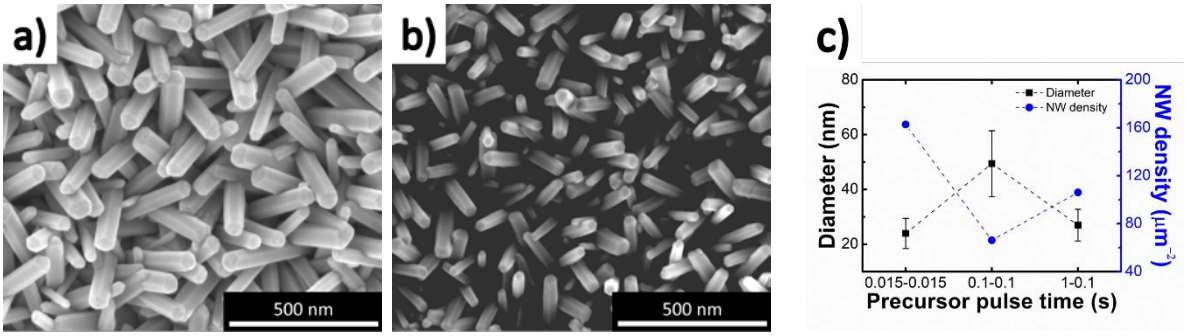

Figure 7. SEM images of the effect of the precursors pulse time on the growth of ZNO NWs for (a) S4 and (b) S5. (c) Comparison of the roughness and NW density for S3, S4 and S5.

Number of ALD deposition cycles

The effect of the number of cycles was studied with samples S6 (Figure 8a) and S7 (Figure 8b), where a lower and higher number of deposition cycles respectively were used compared to S4 (Figure 5a). A comparison of the surface roughness and seed density between these samples is shown in Figure 8c. The thickness of the seed layer increases with the number of cycles. As shown by Chaaya et al.,[49] the seed layer roughness rises with increasing thickness, which in turn increases the variability in the orientation of the as-grown NWs.[14, 35] The AFM images show that these seed layers had a similar microstructure but quite different surface roughness, with a three-fold increase between S6 and S7. The roughness increased with the number of cycles, as shown in Figure 8c. This effect was coupled with an increase in the granular features size as revealed by the line profiles. The line profiles also showed a significantly different microstructure, which was homogeneous for S6 but more irregular for S7. Both seed layers had defined peak features in their line profiles, indicative of granular features in the seed layer. However, the heights and widths of the peaks are different in scale. Considering the seed density (Figure 8c), it was shown that increasing the number of cycles led to a decrease of the seed density of more than half, with the values going from ~173 μm^{-2} for S6 to ~78 for S7 μm^{-2}. This effect proved as well that a higher number of cycles is tied to larger granular features size, as a higher granular feature sizes will lead to a lower seed density.

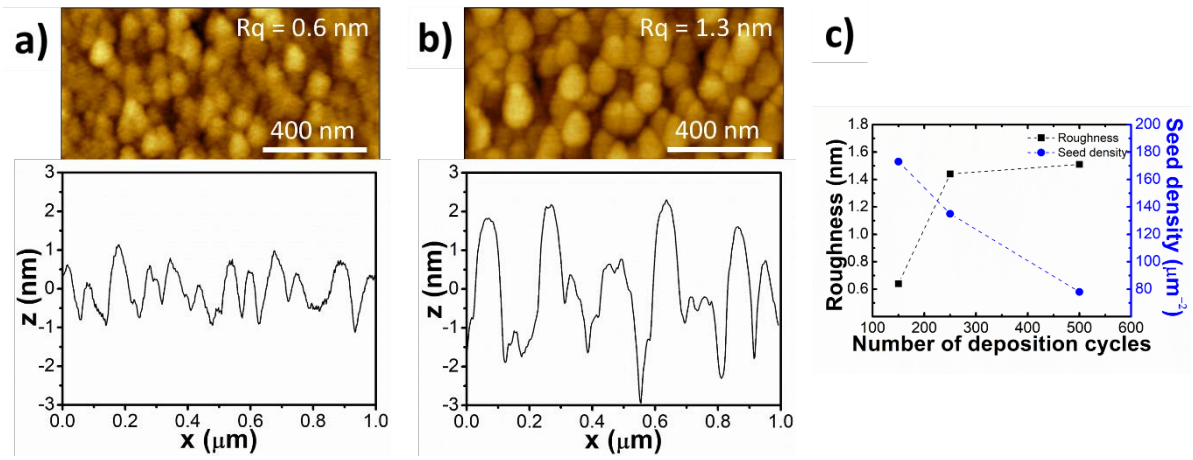

Figure 8. AFM micrographs and line profiles of (a) S6 and (b) S7 in which the influence of the number of deposition cycles was studied. (c) Comparison of roughness values and seed density obtained from the AFM images.

FESEM micrographs of the NWs grown on samples S6 and S7 are shown in Figure 8a,b respectively. A comparison of NW diameter and density between samples S4, S6 and S7 is shown in Figure 9c. There is a clear difference in the variation of orientations of the NWs between both samples. NWs grown on the seed layer with the lower number of cycles had more vertically orientated NWs and a small size distribution granted by the low surface roughness and adequate topography of the seed layer S6. In comparison, NWs grown on S7 had larger diameters (44.3 nm) than those in S6 (38.9 nm), resulting from the larger granular feature sizes, but similar to that of S4 (49.41 nm). The NWs grown on S7 were oriented at a wide range of angles as a result of the higher value of roughness and irregular topography resulting from increased the number of ALD deposition cycles. The NW density decreased as the number of cycles increased due to the surface roughness of the seed layers increased. This increased the randomness of the NW orientation, which decreased the density of NWs, lowering it from 80.1 μm^{-2} for S6 to 41.5 μm^{-2} for S7. Comparing the influence of the number of ALD deposition cycles with the rest of the seed layer deposition parameters, it was demonstrated that this parameter enables a higher degree of control over the growth of the ZnO NWs.

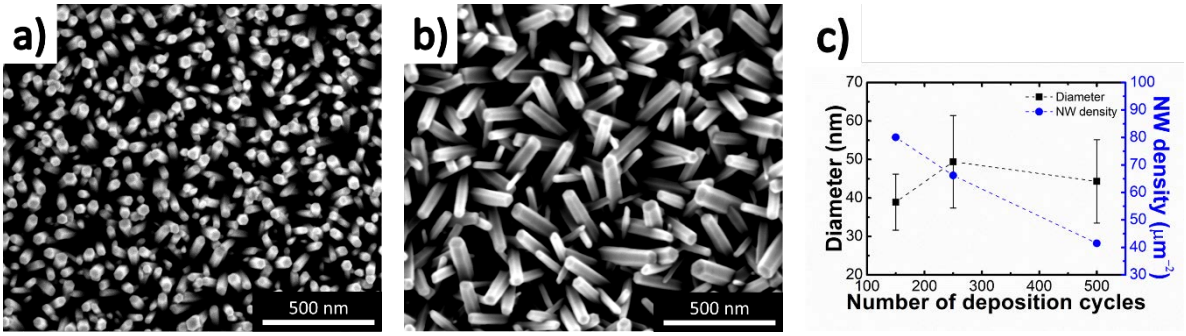

Figure 9. SEM investigations of the effect of the number of ALD deposition cycles on the growth of ZNO NWs for (a) S6 and (b) S7. (c) Comparison of the roughness and NW density for S4, S6 and S7.

Precursor purge times

The precursor purge times in the ALD process also have an important effect on the final properties of the seed layer deposited. Here the purge times were tuned for sample S8 while keeping the deposition temperature at 280ºC on the basis of the work of Park et al.[50] The purge time for DEZ does not critically modify the final properties of the seed layer and, thus, for a higher throughput, it is desirable to be kept as short as possible while being sufficient to allow complete chemisorption of the precursor (in the range of 3 to 20 seconds, depending on the deposition temperature). In contrast, the purge time of the oxidant is a critical factor. If it is too long, desorption will occur, hindering the growth of the atomic layers (desorption is promoted by temperature). However, if it is too short, the chemical reactions between oxidant and DEZ will not fully take place, leaving unreacted precursor on the seed layer. This sensitivity to the oxidant purge time means that it must be finely tuned according to the deposition temperature in order to avoid desorption and accumulation of unreacted precursors. Typical purge times vary from 5 to 30 seconds. The microstructure of sample S8 (Figure 10a) was similar to that of S4 and the parameters are compared in Table 2. The roughness of S8 was notably lower than S4, suggesting the seeding of a better vertical alignment of the NWs grown on S8 compared to S4. The line profile for S8 shows a regular topography and a seed density (~137 μm^{-2}) similar to S4

(~135 μm^{-2}). Thus, by tuning the purge times it is possible to control the roughness of the seed layers while maintaining other properties.

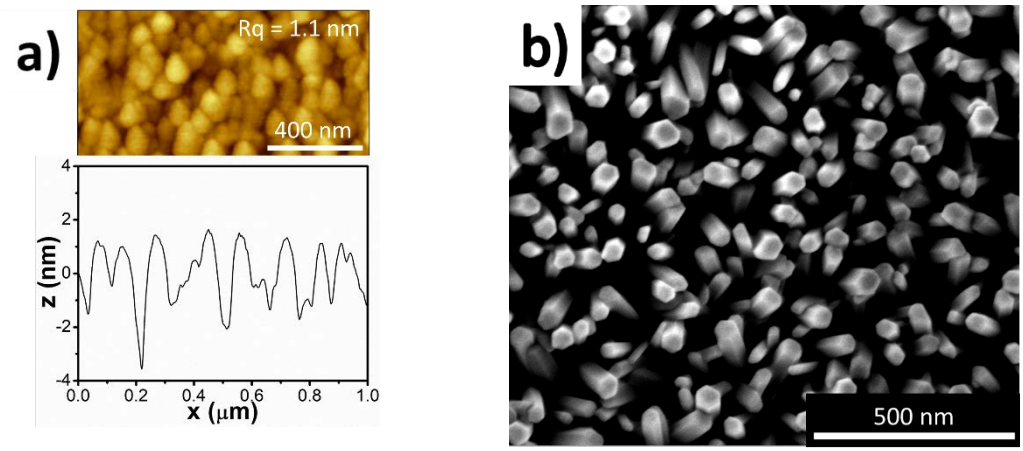

Figure 10. (a) AFM micrograph and line profile of S8 in which the influence of the purge times was studied. (b) FESEM imaging of S8.

The effect of tuning the purge time on the growth of NWs (sample S8) is shown in Figure 10b. The NWs obtained on this seed layer have a slightly smaller average diameter that those grown on S4 (49.4 nm compared to 45.7 nm). However, the NW density of S8 (~98 μm^{-2}) was notably higher than for S4 (~66 μm^{-2}), which is attributed to the lower surface roughness of the seed layer. This, in turn, explains the more uniform orientation of the NWs grown on S8, as opposed to those grown on S4, for which their alignment was varied.

Table 2. Summary of the results obtained from AFM and FESEM analyses performed on samples S4 and S8. The pulse and purge sequences for these samples is shown in Table 1.

Sample	Roughness (nm)	NW diameter (nm)	Seed density (μm^{-2})	NW density (μm^{-2})
S4	1.4	49.4 ±12.0	135.0	66.2
S8	1.1	45.7±9.9	137.3	98.1

Relationship between seed layer microstructure and NW density

Figure 11 shows the relationship between the seed density of the seed layers and the NW density. This shows an approximately linear relationship between the seed density of the seed layers and the NW density, indicating a relationship between the granular features of the seed layer and the nucleation of NWs. The slope of this linear fit is approximately 0.5, suggesting that half of the seeds of the seed layers serve as nucleation points for the NWs for the chemical bath deposition conditions used in this work. The explanation for this lies in the relation between seed density and lateral growth: the lower the seed density is, the less suppressed the lateral growth is, leading to larger NW diameters. Finally, as shown previously, larger NW diameters provide lower NW densities.

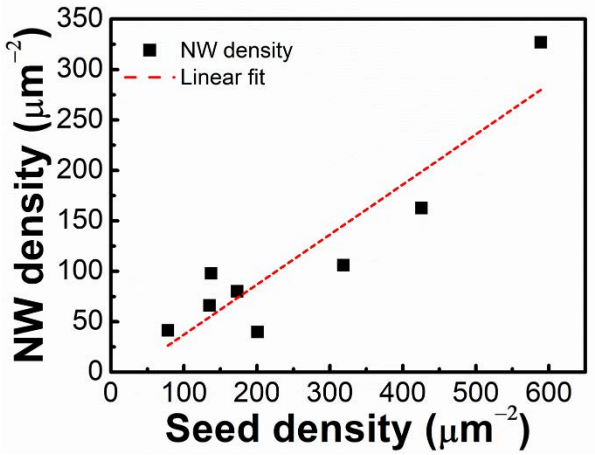

Figure 11. Graph showing the direct relationship between seed density and NW density.

Crystallography of the NWs

The typical morphology and crystallinity of the as-grown NWs was studied by transmission electron microscopy (TEM), Figure 12. The NWs were detached from the Si substrate by scraping them to a copper TEM grid using IPA and a razor. Figure 12a shows an example of a high-resolution TEM (HRTEM) image of an as-grown NW, while the inset depicts the tip of the NW. The HRTEM shows the NWs were single crystalline and their preferred growth orientation was parallel to the [0 0 1]. A selected area electron diffraction (SAED) pattern of this NW is presented in Figure 12b. The diffraction pattern

combined with the HRTEM data clearly demonstrate that the as-grown NWs are single crystal wurtzite phase ZnO NWs. These results suggest that the crystallinity of our ZnO NWs are independent of the seed layer deposition parameters. Furthermore, the HRTEM data combined with SEM analysis demonstrated that the dimensions and orientations of these NWs can be fully controlled by fine-tuning the seed layer deposition parameters.

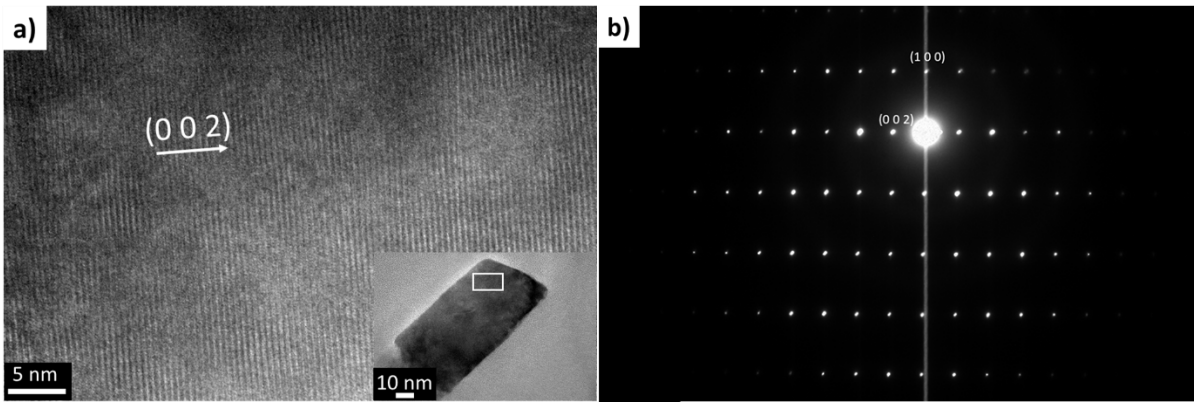

Figure 12. (a) HRTEM image of a ZnO NW and (b) the correspondent diffraction pattern.

Conclusion

Textured ZnO seed layers were deposited on Si (1 0 0) substrates using an ALD system to nucleate the growth of NWs *via* chemical bath deposition. The influence of the different seed layer deposition parameters (pulse and purge time, temperature and number of ALD deposition cycles) were systematically studied to understand the seed layer structural properties and its relationship with the morphology of the as-grown ZnO NWs. It was demonstrated that the seed layer texture and seed density can be controlled by tuning the seed layer deposition parameters and that the uniformity of the orientation of the NWs with respect to the substrate is dependent on the seed layer texture. Adjusting the number of ALD deposition cycles was proven to be the best way to control the roughness and seed size of the seed layers, thus enabling a higher degree of control over the NW size and orientation than the rest of the seed layer deposition parameters. A direct relationship between seed density and NW density was established, which suggests that approximately 50% of the granular

features of the studied seed layers served as nucleation centres for the NW growth with the chemical bath deposition conditions stablished in this work. Finally, it was demonstrated by HRTEM and SAED that the ZnO NWs exhibited a single crystal wurtzite phase.

ORCID

Alejandro Galan Gonzalez: 0000-0002-8217-7445

Andrew J. Gallant: 0000-0002-2040-653X

Dagou Zeze: 0000-0002-6596-5490

Del Atkinson: 0000-0002-9438-7407

Notes

The authors declare no competing financial interests.

Acknowledgments. The project leading to this application has received funding from the European Union's Horizon 2020 research and innovation programme under the Marie Skłodowska-Curie grant agreement No 722176. The authors want to thank M. Cook for his help with the ALD system and C. Pearson for his contributions on the AFM studies. The authors also want to thank B. Mendis for his contributions on the TEM analyses and C. Robert-Goumet and G. Mounier for the XPS measurements performed. The authors are grateful to F. Alkhalil at PragmatIC Printing Ltd. for critical review of this work.

References

1. Barth, S.; Hernandez-Ramirez, F.; Holmes, J. D.; Romano-Rodriguez, A., Synthesis and Applications of One-Dimensional Semiconductors. *Prog Mater Sci.* **2010,** *55*, 563-627.

2. Kolodziejczak-Radzimska, A.; Jesionowski, T., Zinc Oxide-from Synthesis to Application: A Review. *Materials* **2014,** *7*, 2833-2881.
3. Janotti, A.; Van de Walle, C. G., Fundamentals of Zinc Oxide as a Semiconductor. *Rep. Prog. Phys.* **2009,** *72*.
4. Kozhummal, R.; Yang, Y.; Guder, F.; Hartel, A.; Lu, X.; Kucukbayrak, U. M.; Mateo-Alonso, A.; Elwenspoek, M.; Zacharias, M., Homoepitaxial Branching: An Unusual Polymorph of Zinc Oxide Derived from Seeded Solution Growth. *ACS Nano* **2012,** *6*, 7133-7141.
5. Xu, S.; Wang, Z. L., One-Dimensional Zno Nanostructures: Solution Growth and Functional Properties. *Nano Res.* **2011,** *4*, 1013-1098.
6. Chang, Y.-H.; Wang, S.-M.; Liu, C.-M.; Chen, C., Fabrication and Characteristics of Self-Aligned Zno Nanotube and Nanorod Arrays on Si Substrates by Atomic Layer Deposition. *J Electrochem Soc.* **2010,** *157*, 236-241.
7. Chu, D.; Masuda, Y.; Ohji, T.; Kato, K., Formation and Photocatalytic Application of Zno Nanotubes Using Aqueous Solution. *Langmuir* **2010,** *26*, 2811-5.
8. Wang, Z. L., Zno Nanowire and Nanobelt Platform for Nanotechnology. *Mater Sci Eng R Rep* **2009,** *64*, 33-71.
9. Lv, Y.; Zhang, Z.; Yan, J.; Zhao, W.; Zhai, C.; Liu, J., Growth Mechanism and Photoluminescence Property of Hydrothermal Oriented Zno Nanostructures Evolving from Nanorods to Nanoplates. *J Alloys Compd.* **2017,** *718*, 161-169.
10. Greene, L. E.; Law, M.; Dawud H. Tan; Montano, M.; Goldberger, J.; Somorjai, G.; Yang, P., General Route to Vertical Zno Nanowire Arrays Using Textured Zno Seeds. *Nano Lett.* **2005,** *5*, 1231-1236.
11. Cheng, J. J.; Nicaise, S. M.; Berggren, K. K.; Gradecak, S., Dimensional Tailoring of Hydrothermally Grown Zinc Oxide Nanowire Arrays. *Nano Lett.* **2016,** *16*, 753-9.
12. Wang, N.; Cai, Y.; Zhang, R. Q., Growth of Nanowires. *Mater Sci Eng R Rep* **2008,** *60*, 1-51.
13. Kempa, T. J.; Day, R. W.; Kim, S.-K.; Park, H.-G.; Lieber, C. M., Semiconductor Nanowires: A Platform for Exploring Limits and Concepts for Nano-Enabled Solar Cells. *Energy Environ. Sci.* **2013,** *6*.
14. Fragalà, M. E.; Di Mauro, A.; Cristaldi, D. A.; Cantarella, M.; Impellizzeri, G.; Privitera, V., Zno Nanorods Grown on Ultrathin Zno Seed Layers: Application in Water Treatment. *J. Photochem. Photobiol. A* **2017,** *332*, 497-504.
15. Hamid, S. B. A.; Teh, S. J.; Lai, C. W., Photocatalytic Water Oxidation on Zno: A Review. *Catalysts* **2017,** *7*.
16. Sett, D.; Basak, D., Highly Enhanced H 2 Gas Sensing Characteristics of Co:Zno Nanorods and Its Mechanism. *Sens. Actuator B-Chem.* **2017,** *243*, 475-483.
17. Liu, J.; Wu, W.; Bai, S.; Qin, Y., Synthesis of High Crystallinity Zno Nanowire Array on Polymer Substrate and Flexible Fiber-Based Sensor. *ACS Appl Mater Interfaces.* **2011,** *3*, 4197-200.
18. Tan, C. H.; Tan, S. T.; Lee, H. B.; Ginting, R. T.; Oleiwi, H. F.; Yap, C. C.; Jumali, M. H. H.; Yahaya, M., Automated Room Temperature Optical Absorbance Co Sensor Based on in-Doped Zno Nanorod. *Sens. Actuator B-Chem.* **2017,** *248*, 140-152.
19. Nayeri, F. D.; Soleimani, E. A.; Salehi, F., Synthesis and Characterization of Zno Nanowires Grown on Different Seed Layers: The Application for Dye-Sensitized Solar Cells. *Renew Energy* **2013,** *60*, 246-255.
20. Li, S.; Zhang, P.; Wang, Y.; Sarvari, H.; Liu, D.; Wu, J.; Yang, Y.; Wang, Z.; Chen, Z. D., Interface Engineering of High Efficiency Perovskite Solar Cells Based on Zno Nanorods Using Atomic Layer Deposition. *Nano Res.* **2016,** *10*, 1092-1103.

21. Zeng, J. H.; Jin, B. B.; Wang, Y. F., Facet Enhanced Photocatalytic Effect with Uniform Single-Crystalline Zinc Oxide Nanodisks. *Chem. Phys. Lett.* **2009,** *472*, 90-95.
22. Wang, G.; Yang, X.; Qian, F.; Zhang, J. Z.; Li, Y., Double-Sided Cds and Cdse Quantum Dot Co-Sensitized Zno Nanowire Arrays for Photoelectrochemical Hydrogen Generation. *Nano Lett.* **2010,** *10*, 1088-92.
23. Kuriakose, S.; Satpati, B.; Mohapatra, S., Enhanced Photocatalytic Activity of Co Doped Zno Nanodisks and Nanorods Prepared by a Facile Wet Chemical Method. *Phys Chem Chem Phys* **2014,** *16*, 12741-9.
24. Willander, M.; Nur, O.; Zhao, Q. X.; Yang, L. L.; Lorenz, M.; Cao, B. Q.; Zuniga Perez, J.; Czekalla, C.; Zimmermann, G.; Grundmann, M., et al., Zinc Oxide Nanorod Based Photonic Devices: Recent Progress in Growth, Light Emitting Diodes and Lasers. *Nanotechnology* **2009,** *20*, 332001.
25. Isakov, I.; Panfilova, M.; Sourribes, M. J. L.; Warburton, P. A., Growth of Zno and Znmgo Nanowires by Au-Catalysed Molecular-Beam Epitaxy. *Phys. Status Solidi C* **2013,** *10*, 1308-1313.
26. Ruhle, S.; Shalom, M.; Zaban, A., Quantum-Dot-Sensitized Solar Cells. *Chemphyschem* **2010,** *11* (11), 2290-304.
27. Xia, X.; Tu, J.; Zhang, Y.; XiuliWang; Gu, C.; Zhao, X.-b.; JinFan, H., High-Quality Metal Oxide Core-Shell Nanowire Arrays on Conductive Substrates for Electrochemical Energy Storage. *ACS Nano* **2012,** *6* (6), 5531.
28. Strano, V.; Urso, R. G.; Scuderi, M.; Iwu, K. O.; Simone, F.; Ciliberto, E.; Spinella, C.; Mirabella, S., Double Role of Hmta in Zno Nanorods Grown by Chemical Bath Deposition. *J. Phys. Chem. C* **2014,** *118*, 28189-28195.
29. Parize, R.; Garnier, J.; Chaix-Pluchery, O.; Verrier, C.; Appert, E.; Consonni, V., Effects of Hexamethylenetetramine on the Nucleation and Radial Growth of Zno Nanowires by Chemical Bath Deposition. *J. Phys. Chem. C* **2016,** *120*, 5242-5250.
30. Qu, Y.; Huang, X.; Li, Y.; Lin, G.; Guo, B.; Song, D.; Cheng, Q., Chemical Bath Deposition Produced Zno Nanorod Arrays as an Antireflective Layer in the Polycrystalline Si Solar Cells. *J Alloys Compd.* **2017,** *698*, 719-724.
31. Jung, J.; Myoung, J.; Lim, S., Effects of Zno Nanowire Synthesis Parameters on the Photovoltaic Performance of Dye-Sensitized Solar Cells. *Thin Solid Films* **2012,** *520* (17), 5779-5789.
32. Verrier, C.; Appert, E.; Chaix-Pluchery, O.; Rapenne, L.; Rafhay, Q.; Kaminski-Cachopo, A.; Consonni, V., Effects of the Ph on the Formation and Doping Mechanisms of Zno Nanowires Using Aluminum Nitrate and Ammonia. *Inorg Chem* **2017,** *56*, 13111-13122.
33. Kim, H.; Wang, Z.; Hedhili, M. N.; Wehbe, N.; Alshareef, H. N., Oxidant-Dependent Thermoelectric Properties of Undoped Zno Films by Atomic Layer Deposition. *Chem. Mater.* **2017,** *29*, 2794-2802.
34. Ladanov, M.; Algarin-Amaris, P.; Villalba, P.; Emirov, Y.; Matthews, G.; Thomas, S.; Ram, M. K.; Kumar, A.; Wang, J., Effects of the Physical Properties of Atomic Layer Deposition Grown Seeding Layers on the Preparation of Zno Nanowires. *J. Phys. Chem. Solids* **2013,** *74*, 1578-1588.
35. Bielinski, A. R.; Kazyak, E.; Schlepütz, C. M.; Jung, H. J.; Wood, K. N.; Dasgupta, N. P., Hierarchical Zno Nanowire Growth with Tunable Orientations on Versatile Substrates Using Atomic Layer Deposition Seeding. *Chem. Mater.* **2015,** *27*, 4799-4807.
36. Johnson, R. W.; Hultqvist, A.; Bent, S. F., A Brief Review of Atomic Layer Deposition: From Fundamentals to Applications. *Mater. Today* **2014,** *17*, 236-246.

37. George, S. M., Atomic Layer Deposition. An Overview. *Chemical Reviews* **2010,** *110*, 111-131.
38. Weber, M.; Coy, E.; Iatsunskyi, I.; Yate, L.; Miele, P.; Bechelany, M., Mechanical Properties of Boron Nitride Thin Films Prepared by Atomic Layer Deposition. *CrystEngComm* **2017,** *19* (41), 6089-6094.
39. Weber, M. J.; Verheijen, M. A.; Bol, A. A.; Kessels, W. M., Sub-Nanometer Dimensions Control of Core/Shell Nanoparticles Prepared by Atomic Layer Deposition. *Nanotechnology* **2015,** *26* (9), 094002.
40. Song, J.; Lim, S., Effect of Seed Layer on the Growth of Zno Nanorods. *Journal of Physical Chemistry C* **2007,** *111* (2), 596-600.
41. Liu, J.; She, J.; Deng, S.; Chen, J.; Xu, N., Ultrathin Seed-Layer for Tuning Density of Zno Nanowire Arrays and Their Field Emission Characteristics. *Journal of Physical Chemistry C* **2008,** *112* (31), 11685-11690.
42. Chen, S.-W.; Wu, J.-M., Nucleation Mechanisms and Their Influences on Characteristics of Zno Nanorod Arrays Prepared by a Hydrothermal Method. *Acta Materialia* **2011,** *59*, 841-847.
43. Szabó, Z.; Cora, I.; Horváth, Z.; Volk, J.; Baji, Z., Hierarchical Oxide Nanostructures Fabricated with Atomic Layer Deposition and Hydrothermal Growth. *Nano-Structures & Nano-Objects* **2018,** *13*, 100-108.
44. Jeong, J. S.; Lee, J. Y., Investigation of Initial Growth of Zno Nanowires and Their Growth Mechanism. *Nanotechnology* **2010,** *21*, 475603.
45. Rogé, V.; Bahlawane, N.; Lamblin, G.; Fechete, I.; Garin, F.; Dinia, A.; Lenoble, D., Improvement of the Photocatalytic Degradation Property of Atomic Layer Deposited Zno Thin Films: The Interplay between Film Properties and Functional Performances. *J. Mater. Chem. A* **2015,** *3*, 11453-11461.
46. Pung, S. Y.; Choy, K. L.; Hou, X.; Shan, C., Preferential Growth of Zno Thin Films by the Atomic Layer Deposition Technique. *Nanotechnology* **2008,** *19*, 435609.
47. Tian, J.-L.; Zhang, H.-Y.; Wang, G.-G.; Wang, X.-Z.; Sun, R.; Jin, L.; Han, J.-C., Influence of Film Thickness and Annealing Temperature on the Structural and Optical Properties of Zno Thin Films on Si (100) Substrates Grown by Atomic Layer Deposition. *Superlattices and Microstructures* **2015,** *83*, 719-729.
48. Weckman, T.; Laasonen, K., Atomic Layer Deposition of Zinc Oxide: Diethyl Zinc Reactions and Surface Saturation from First-Principles. *J. Phys. Chem. C* **2016,** *120*, 21460-21471.
49. Abou Chaaya, A.; Viter, R.; Bechelany, M.; Alute, Z.; Erts, D.; Zalesskaya, A.; Kovalevskis, K.; Rouessac, V.; Smyntyna, V.; Miele, P., Evolution of Microstructure and Related Optical Properties of Zno Grown by Atomic Layer Deposition. *Beilstein J Nanotechnol* **2013,** *4*, 690-8.
50. Park, H. K.; Yang, B. S.; Park, S.; Kim, M. S.; Shin, J. C.; Heo, J., Purge-Time-Dependent Growth of Zno Thin Films by Atomic Layer Deposition. *J Alloys Compd.* **2014,** *605*, 124-130.